Supplementary Information

to the article entitled:

Responsive materials: A novel design for enhanced machine-augmented composites

Ehsan Bafekrpour[1], Andrey Molotnikov[1], James C. Weaver[2], Yves Brechet[3], Yuri Estrin[1,4]*

[1]*Centre for Advanced Hybrid Materials, Department of Materials Engineering, Monash University, Clayton, Victoria 3800, Australia*

[2]*Wyss Institute for Biologically Inspired Engineering, Harvard University, Cambridge, Massachusetts 02138, USA*

[3]*Phelma, INP Grenoble, Domaine Universitaire, St Martin d'Heres,-France*

[4]*Laboratory of Hybrid Nanostructured Materials, Moscow Institute of Steel and Alloys, Leninsky prosp. 4, Moscow 119049, Russia*

Corresponding author, Email address: yuri.estrin@monash.edu

Tel: (+61) 3 9905 9599, Fax: (+61) 3 9905 4940

Contents

1. Fabrication of converter machines and MACs by 3D printing

As suggested by Hawkins et al.[1], an individual machine is made up by two walls and two flanges, cf. Fig. 1 of the main text, which depicts a stand-alone Z-machine (a) and a Z-MAC (b). Both the individual machines and the MACs studied in this work were produced through additive manufacturing. In the choice of the particular architectures used, guidance was provided by finite element modelling, see below. The materials used for the machines and the matrix were also chosen in accordance with the optimised ratio of their elastic moduli suggested by FEM analysis. Polymers based on UV curable urethanes and acrylates offer the possibility of tailoring the elastic properties over a broad range by varying the mixing ratios of rigid and flexible phases. This made it possible to implement, in a real MAC, two grades of a polymer with strongly contrasting elastic properties, as suggested by FEM simulations. The machines and MACs were built with a Stratasys® Connex500 multimaterial 3D printer. The machine to matrix stiffness ratio was tuned by blending a stiff elastomer (VeroWhite®), which simulates conventional thermoplastics, with another, rubber-like one (TangoPlus® or TangoBlackPlus®). The "3D ink" precursor used was a mixture of acrylate and urethane monomers and oligomers, cross-linkers, and photoinitiators in a liquid form. Immediately after these inks were ejected from the print heads, they were polymerized with UV light. The inks were deposited in a pixel-by-pixel fashion, so that fine shape control was achieved, with a spatial resolution of ca. 30 mm in the z-direction. Materials with different intermediate levels of stiffness were obtained by printing juxtaposed pixels of the two "rigid" and "flexible" extremes in different ratios.

In the MACs with the geometry produced using a multi-material 3D printer, the individual converter machines embedded in a softer matrix were 10 mm apart, cf. Fig. 1 of the main text. This distance was shown to be adequate to allow the movement of the machine walls. The overall dimensions of the MACs fabricated were 74mm×20mm×24mm. The

printer was operated in the digital material print mode with horizontally deposited layers measuring ca. 30 µm in thickness. Using this approach, the MACs were fabricated by simultaneously depositing two different materials for the machines and the matrix. Examples of the 3D printed MACs are shown in Fig. S1.

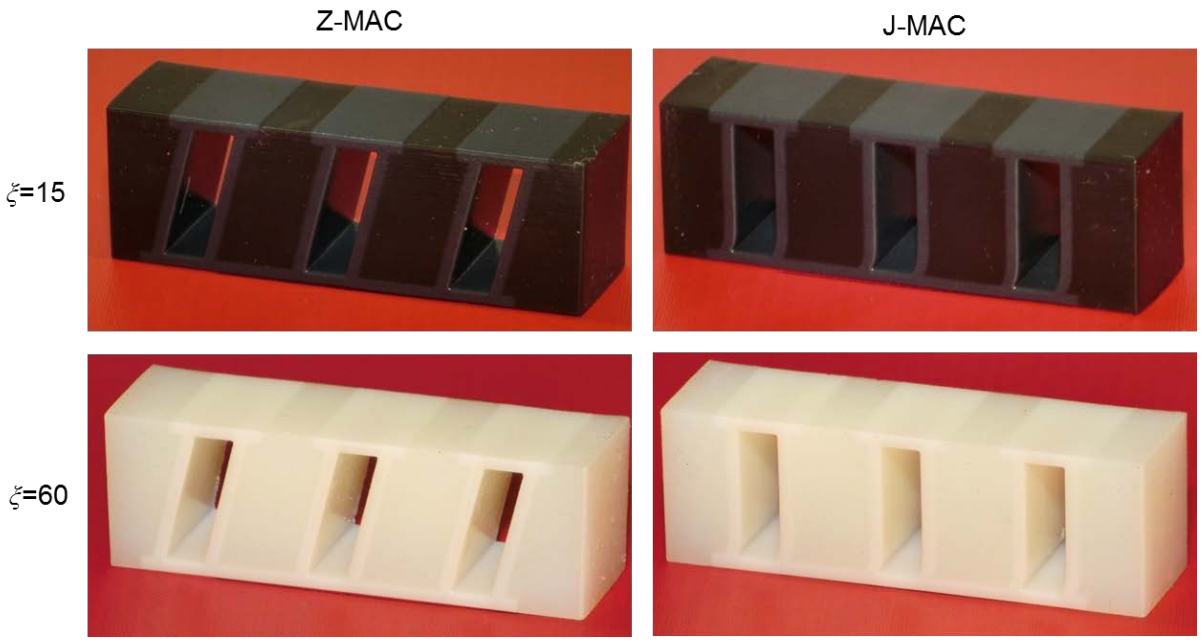

Figure S1. MACs fabricated by means of multi-material 3D printing with different elastomer couples. Hawkins' Z-MAC (left) and the modified MAC design, J-MAC (right) are shown. The parameter ξ stands for the ratio of the Young's moduli of the machines and the matrix they are embedded in.

2. Mechanical tests

Mechanical properties of the polymers used in making the stand-alone machines and the MACs were characterised by standard mechanical testing. In particular, the Young's moduli were obtained by tensile tests performed on an Instron 5982 machine equipped with a calibrated 1kN load cell. The tests were carried out in accordance with the ASTM D 638 standard for tensile properties of plastics. They were conducted on dog-bone shaped specimens at a crosshead speed of 1 mm/min at room temperature (22°C). A 10 mm extensometer with a sensitivity of 2.5% mV/V was used to measure the strain in the gauge part of a tensile sample. A pre-load of about 0.5 – 1 N was applied to the samples before commencement of the tests. The samples were deformed to 20% strain and the machine was stopped before failure occurred. The Young's modulus was calculated from the slope of the linear region of the stress-strain curve. Energy absorption of the MACs was investigated using loading and unloading cycles to measure the area of a hysteresis loop obtained, where a quasi-static compression in the displacement control regime with a cross-head speed of 3 mm/min was employed.

3. Measurements of displacement conversion efficiency

The displacement conversion efficiency of stand-alone machines and MACs was examined by applying a (vertical) compressive displacement in a uniaxial compression setup and measuring the resulting (horizontal) shear displacement. However, the expected conversion of vertical displacement into a horizontal one is only possible if it is not hindered by friction between the flanges of a machine (or a composite with the embedded machines) and the platens of the loading device. Therefore, to provide the machines of the kind depicted in Fig. S2 with the freedom to translate vertical displacements into horizontal ones, two identical machines were sandwiched together by placing one on top of the other in a mirrored

arrangement. When compressed, both machines comprising this sandwich produce horizontal movement of a bar separating them in the same direction, as shown in Fig. S2a. The samples were placed between two platens in the testing machine and loaded quasi-statically (at a speed of 3 mm/min) under displacement control. The output data, i.e. the horizontal displacement of the bar, were recorded by an extensometer (Fig.S2) as a measure of the shear displacement produced by the machines in response to normal (vertical) displacement. Prior to the test, the samples were cleaned to remove any supporting material residues from 3D printing. Throughout the test the deformation of the machines was captured by a high-resolution digital camera throughout the test. Composites with the embedded machines (MACs) were tested in a similar way, as illustrated in Fig. S2b. The performance of different MACs was compared based on the conversion efficiency η defined by Equation (2) of the main text.

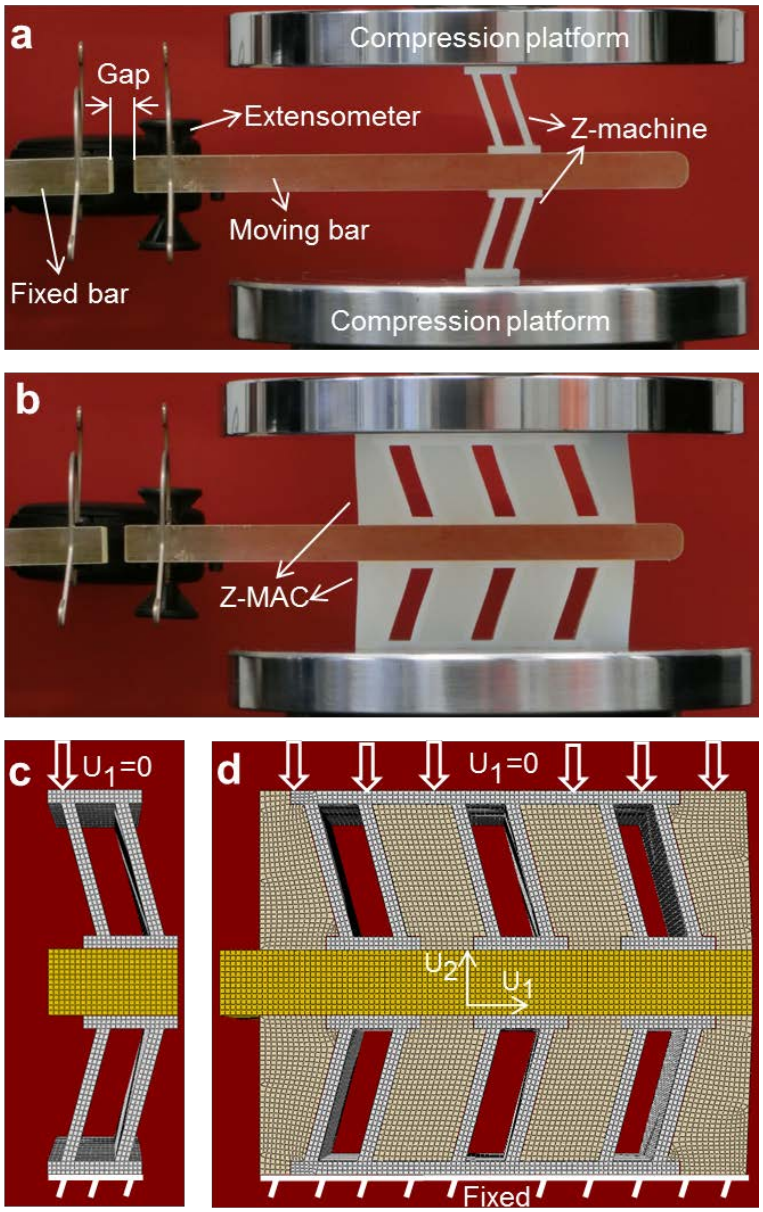

Figure S2. Conversion performance measurements: (a) experimental setup for a pair of Z-machines, (b) experimental setup for a pair of MACs. Figures (c) and (d) show the corresponding finite element models for Z-machines and Z-MACs, respectively. No relative sliding between the converter devices and the platens of the loading machine was assumed (full sticking, $U_1 = 0$).

4. FEM analysis

The conversion performance of Hawkins' Z-machines was investigated by finite element analysis. FEM simulations were also employed for optimisation of machines with regard to displacement conversion performance. The results served as a basis for programs used for 3D printing of machines and MACs using the computer-aided design (CAD) software SolidWorks 2012. For the purposes of displacement conversion, the walls of a Z-machine were tilted in the (x,y) plane, cf. Fig. 1 of the main text. Accordingly, the bending stiffness of a wall in the (x,y) plane (EI_z) should be much lower than that in the (y,z) plane (EI_x): Hence, the inequality

$$EI_z << EI_x \tag{S1}$$

needs to be fulfilled. Here E is the elastic modulus of the wall material and the moments of inertia I_z and I_x are defined as follows:

$$I_z = ec^3/12 \tag{S2}$$

$$I_x = ce^3/12 \tag{S3}$$

where c is the thickness of an angled sidewall and e is the length of the machine in z-direction, cf. Fig. 1. It can thus be seen from equations (S1)-(S3) that Z-machines should be designed such that $c << e$ holds.

Three-dimensional FEM simulations were carried out using the commercial package ABAQUS 6.12-1[2] to evaluate the deformation behaviour and the performance of converter machines and MACs based on them. Hexahedral elements (C3D8) were employed for a static

analysis. The flanges of a simulated machine in contact with a platen of the machine and the middle bar were fixed and a specified compressive vertical displacement was imposed, as shown in Fig. S2c for a pair of Z-machines in the sandwich configuration mentioned above. Similar loading conditions were used for MACs, cf. Fig. S2d, which illustrates the simulated behaviour of a pair of Z-MACs. Perfect adhesion between the two machines or the two MACs of a couple and the middle bar was assumed. In FEM simulations, a convergence analysis was performed, and an acceptable compromise between the accuracy and the CPU time was obtained. In the simulations of the behaviour of the MACs, models consisting of 95,040 elements were employed. The values of the elastic modulus for the machines, $E_{machine}$ = 845 MPa, and the matrix, E_{matrix} =14.5 MPa, obtained from tensile tests were used.

5. Displacement conversion performance of Z-machines

The effect of the initial inclination angle of the Z-machine walls was studied by FEM simulations. The results for wall angles of 45°, 60°, 75°, and 90° presented in Fig. S3 shows the trends observed in these numerical experiments. (The results for the 90° case that did not give rise to horizontal displacements are not shown.). It is seen that the output shear displacement increased with an increase in the wall angle and resulted in better conversion performance of the machines. Among the machines considered, the one with the 75° inclination angle of the walls shows the highest value of the displacement conversion ratio η defined in equation (1). This is consistent with the results of the Hawkins group who demonstrated a continual increase of η with the wall angle[1]. However, one cannot make use of this increase because, as the wall inclination angle reaches 90°, the probability of buckling increases and the performance of Z-machines breaks down at 90°. The maximum input displacement at which buckling of a vertical (90°) wall occurs is estimated according to the classical Euler formula at 0.64 mm. Z-machines with a 75° inclination angle (Z75) favoured

by the Hawkins group do, indeed, appear to be a best option in terms of high displacement conversion performance and buckling prevention, Therefore we studied the displacement conversion performance of Z75 experimentally, following the procedure described above. The corresponding data are presented in Fig. S3, along with the FEM results. A nearly perfect agreement between the FEM prediction and the experimental data was found, thus validating the model.

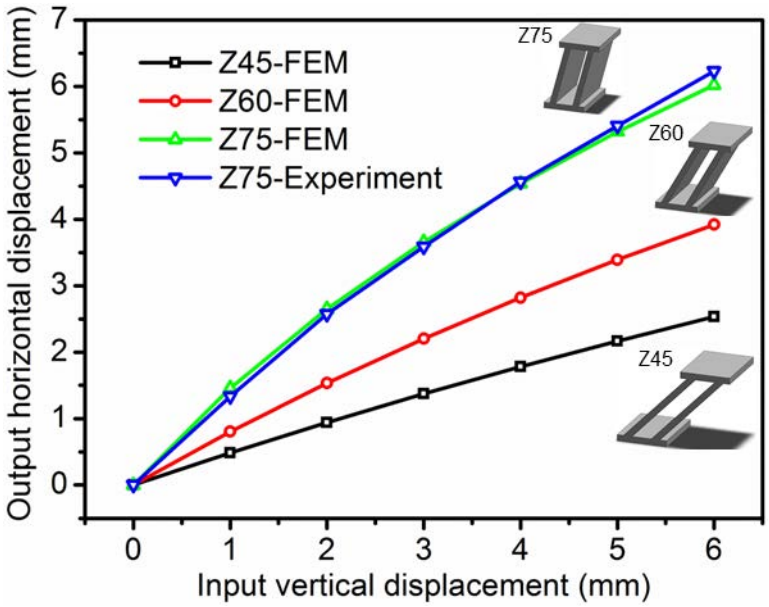

Figure S3. Displacement conversion performance of Z-machines with different wall angles.

6. J-MAC design

The wall shape of the J-machine (Fig. 1c and d of the main text), which we propose as a better version of MAC design, was presented by equation (2). The various shapes corresponding to the different parameter values are shown in Fig. S4.

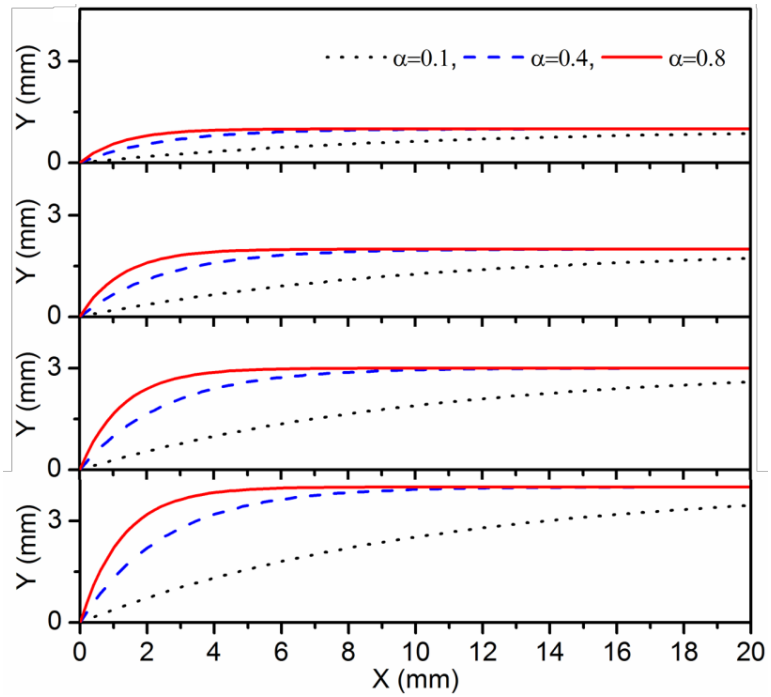

Figure S4. Plots of J-profiles according to equation (2). From top to bottom: y_∞=1 mm, y_∞=2 mm, y_∞=3 mm, y_∞=4 mm. (y_o was set to zero).

Based on the above geometry, J-machines were designed in SolidWorks and then imported into finite element analysis software ABAQUS to calculate the displacement conversion performance. Deformation of J-machines with different shape parameters is presented in Figs. S5-S7.

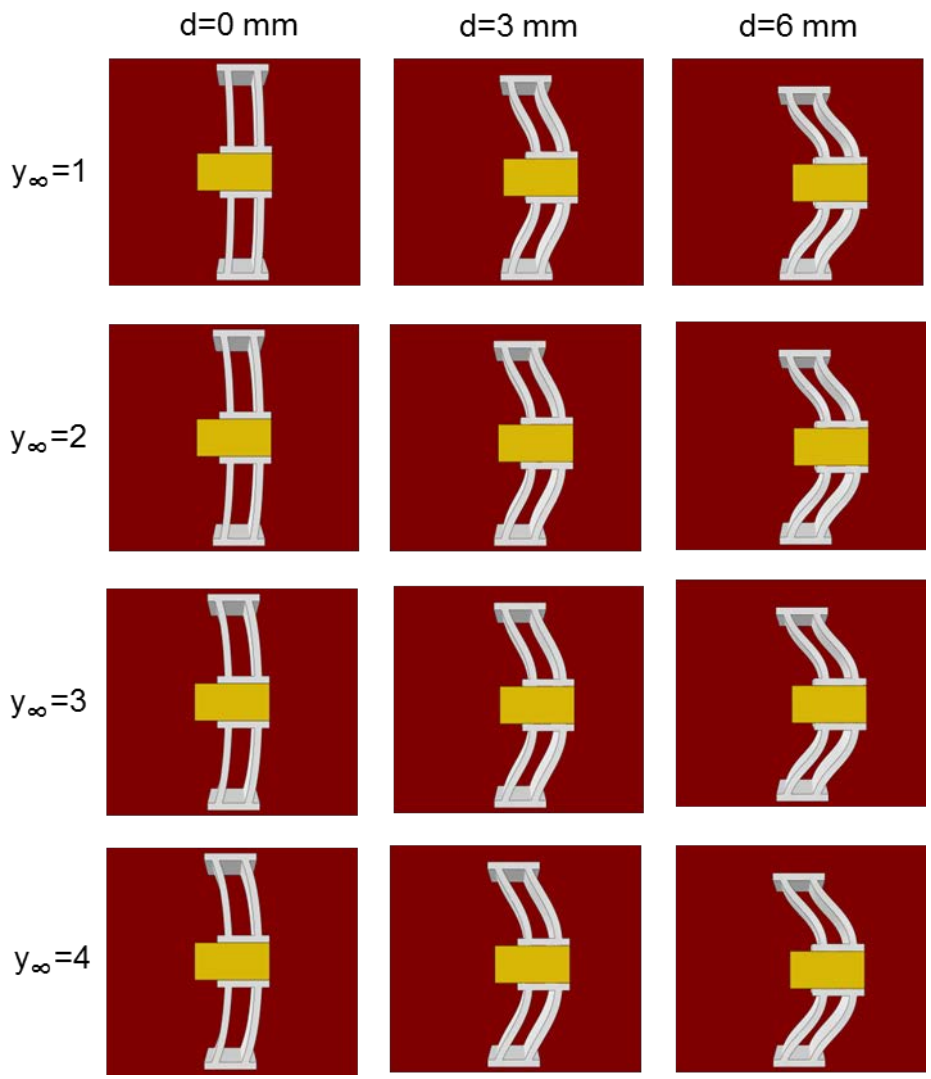

Figure S5. FEM images of J-machines with $\alpha=0.1$ and different y_∞ values for three different levels of vertical displacement d (all y_∞-values in mm).

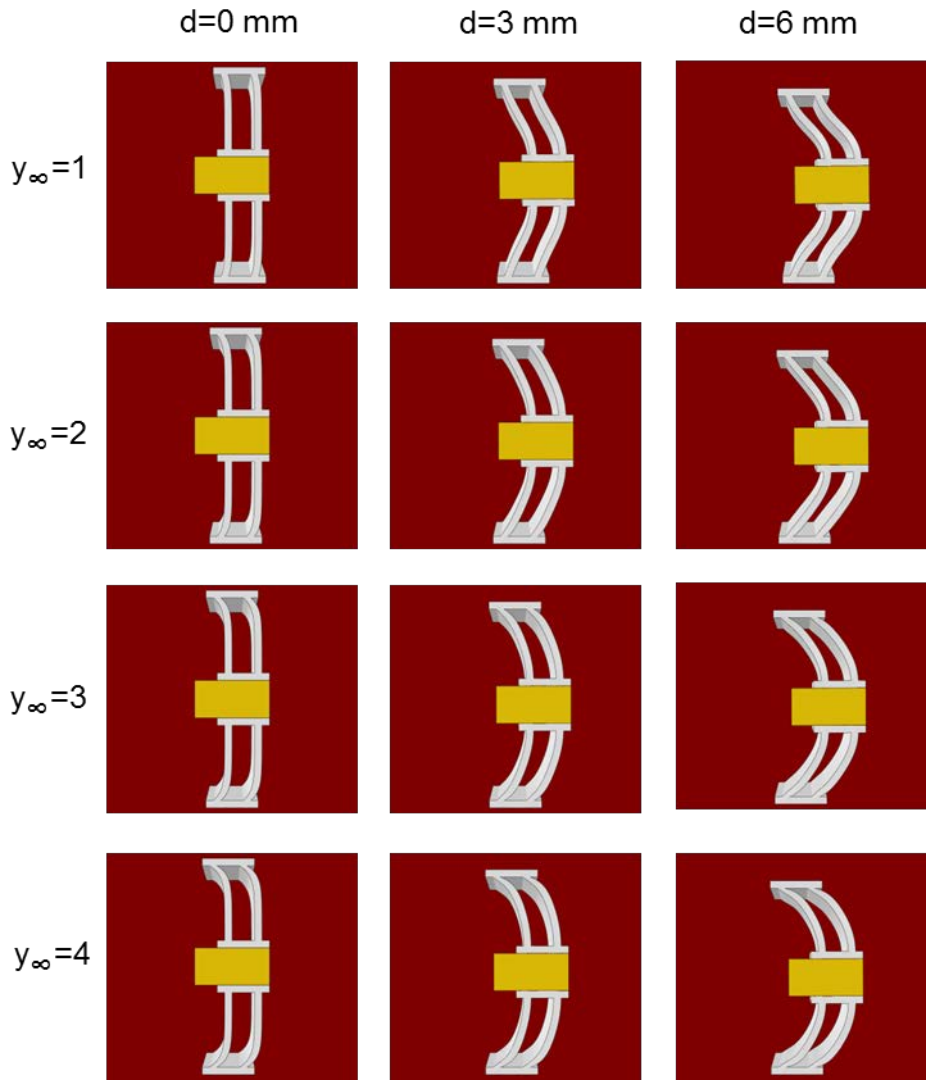

Figure S6. FEM images of J-machines with $\alpha=0.4$ and different y_∞ values for three different levels of vertical displacement d (all y_∞-values in mm).

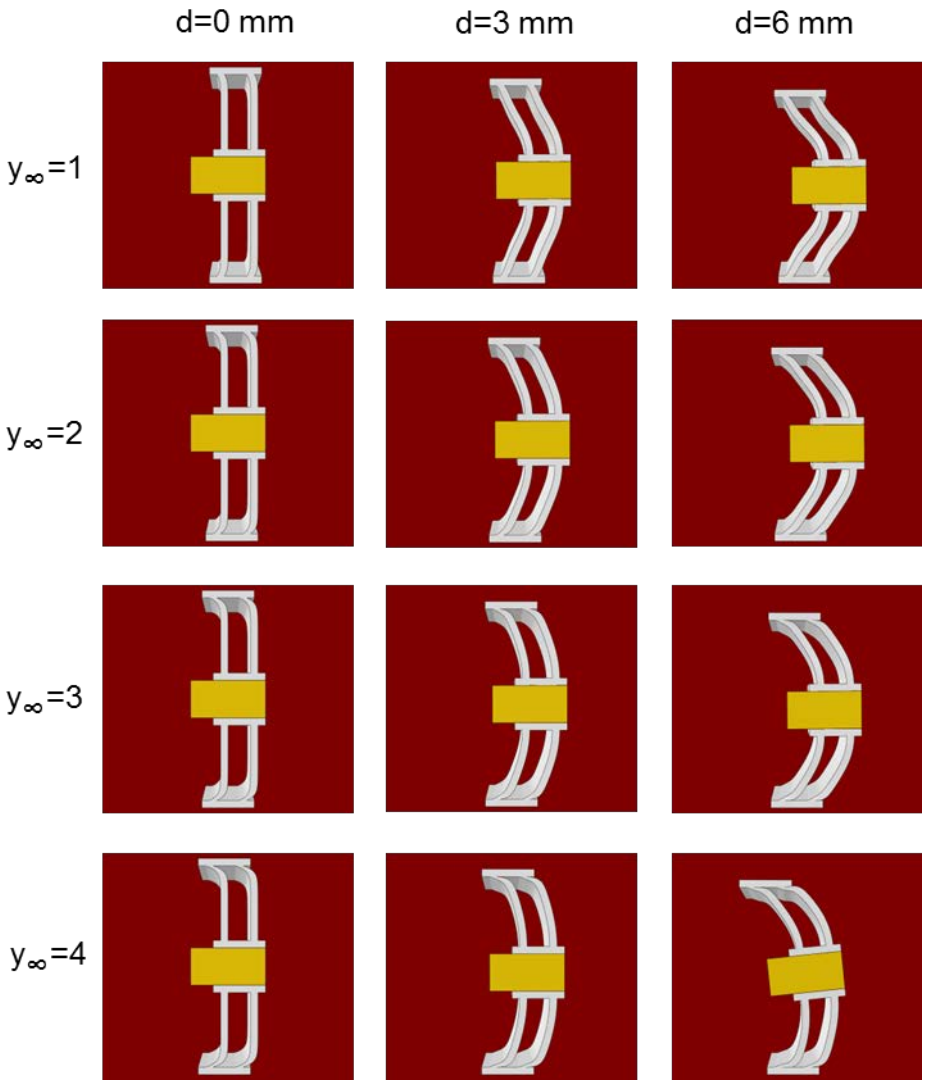

Figure S7. FEM images of J-machines with α=*0.8* and different y_∞ values for three different levels of vertical displacement *d* (all y_∞-values in mm).

FEM analysis showed that the best efficiency of displacement conversion of a J-machine is achieved with the parameter values $y_\infty = 1$ mm and α = 0.8. J-machines based on the optimum parameter set (α = 0.8, $y_\infty = 1$ mm) were 3D printed ($E_{machine}$ = 845 MPa) and their conversion performance experimentally investigated. The photographs taken during three different stages of loading in such experiments are given in Fig. S8.

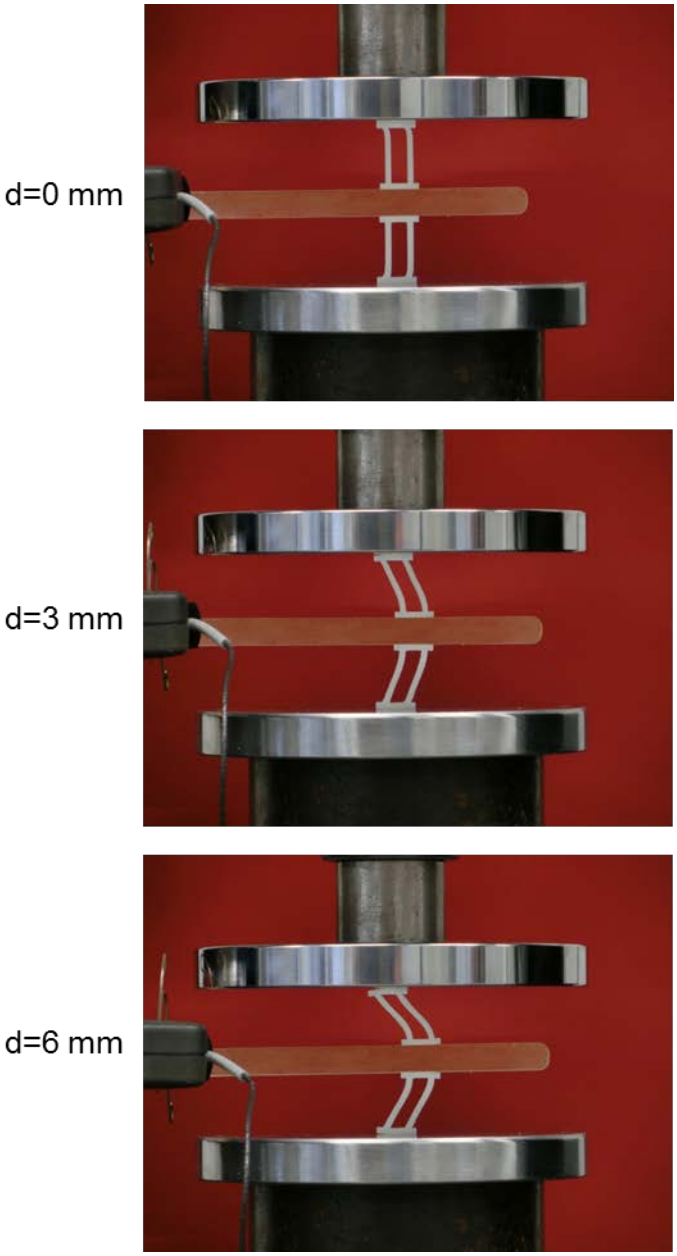

Figure S8. Experimental images of J-machine (α = 0.8, y_∞=1 mm) at three different vertical displacements *d*.

A comparison between the experimental and FEM-simulated response of the J-MAC with ξ =60 to vertical displacement is documented in Fig. S9. The results of the displacement conversion tests on J-MAC with ξ =15 are presented in Fig. S10.

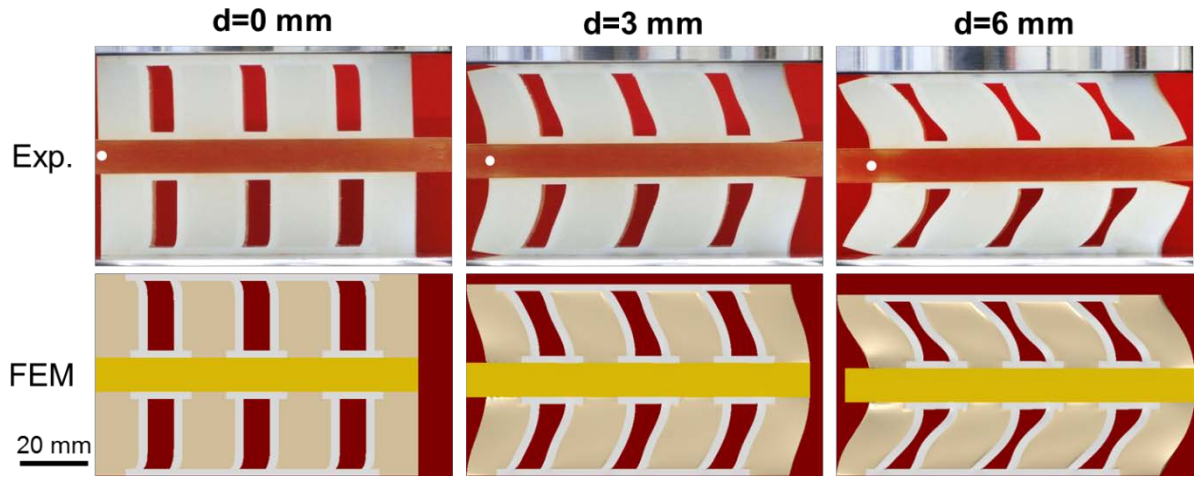

Figure S9. Experimental (top) and FEM (bottom) images of J-MAC with ξ =60 at different values of the input vertical displacement, *d*. The horizontal displacement to the right of the bar sandwiched between the machines can be traced by viewing the displacement of the white marker.

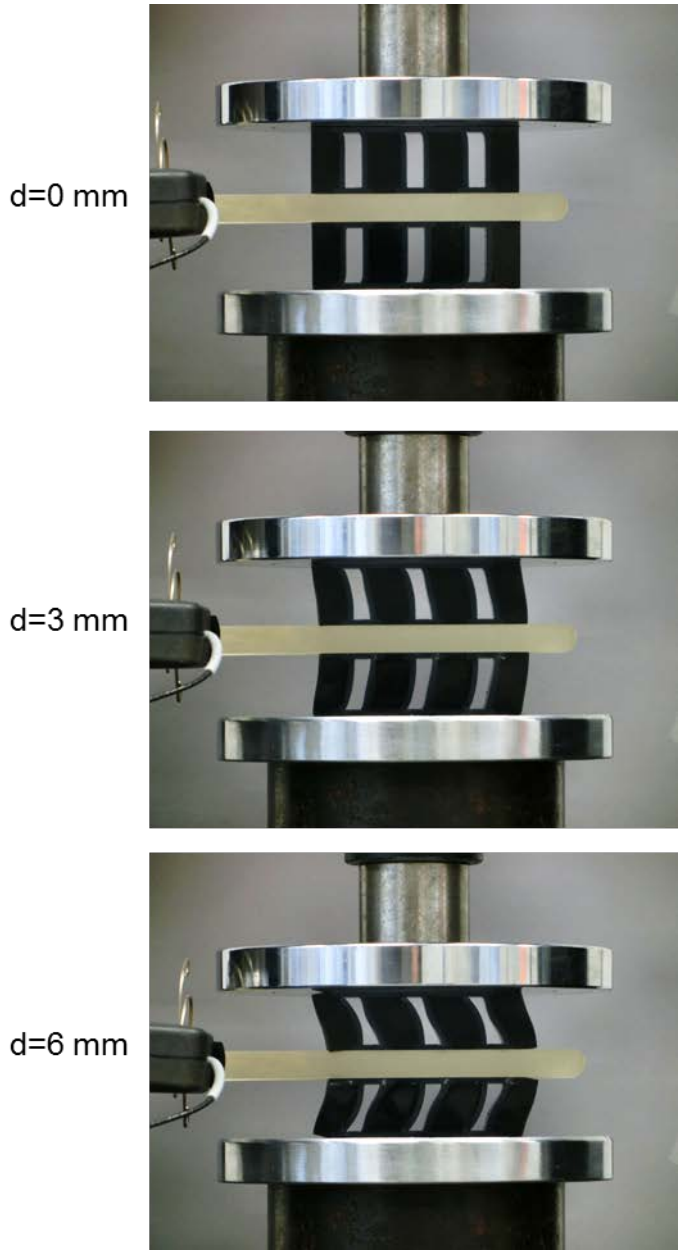

Figure S10. Experimental images of J-MAC with ξ =15 at three different vertical displacements *d*.

7. Compression-conversion MACs

Fig. S11 shows a mechanism designed to produce rotation as a result of compression. As in the other examples of MACs in this paper, they can be positioned in a mirror orientation to each other. When compressive displacements are applied at the top and bottom

disks, the double-disk in the middle responds with rotation, as visualized by the displacements of the black vertical markers in Figs. S11c, e, and g. Additional demonstration of this mechanism is given in Fig. S11d, f, and h where rotation of a horizontal arrow (in green) attached to the double-disk in the middle with respect to another arrow, also in green, which is attached to the bottom disk, is seen in a projection on a horizontal plane.

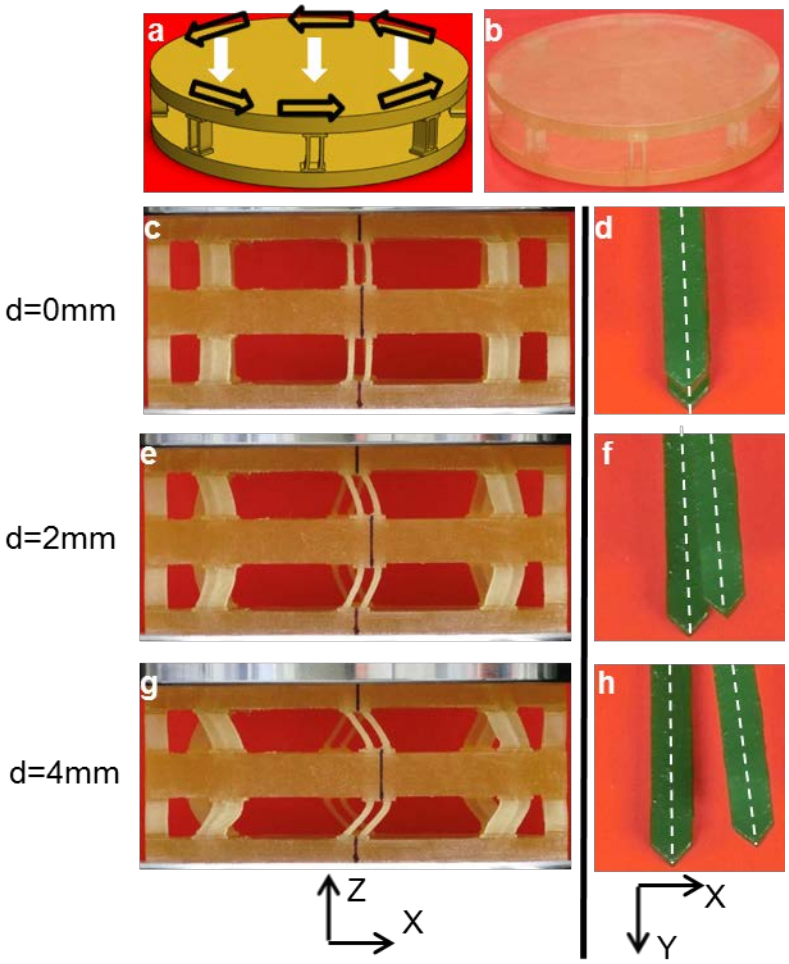

Figure S11. Compression-rotation mechanism: (a) 3D design, (b) 3D printed sample, (c) and (d) *d*=0 mm, (e) and (f) *d*=2 mm, (g) and (h) *d*=4 mm. Photographs (d), (f) and (h) show the projections onto a horizontal plane of horizontal arrows attached to the middle and the bottom disks. Note that in the original configuration the upper arrow was located exactly above the

lower one. The rotation of the middle disks is documented in the occurrence of an angle between the projections of the arrows upon application of vertical displacement.

References

1. Hawkins, G. F. Augmenting the mechanical properties of materials by embedding simple machines. *J. Adv. Mater.* **34,** 16-20 (2002).
2. Abaqus Documentation and User Manual, Version 6.12, Simulia, Dassault Systèmes, (2012).